Organization of Rainfall by an Unstable Jet with an Application to African Waves

R. L. MILLER AND R. S. LINDZEN

Center for Meteorology and Physical Oceanography, Massachusetts Institute of Technology, Cambridge, Massachusetts

(Manuscript received 20 September 1990, in final form 9 December 1991)

ABSTRACT

African waves are believed to originate as shear instabilities, although in certain cases rainfall is organized so that latent heating contributes to wave growth. What determines whether the shear instability can organize rainfall is considered here; in particular, why African waves organize rainfall mainly during the late summer, despite the regular occurrence of shear instability and rainfall throughout the season.

During GATE, moisture convergence by the waves was also largest toward the late summer. It is assumed that an African wave will organize rainfall if it converges moisture—as measured by the ascent at the top of the moist layer—with sufficient amplitude. The wave amplitude is specified at some level beneath the 600-mb African jet, whose instability is a plausible source of the wave. The ascent is calculated using the quasigeostrophic potential vorticity and thermodynamic equations, and depends on the zonal wind separating the unstable jet from the top of the moist layer.

Before turning to the example of the African jet, the more general behavior of the model is considered. In the absence of shear, a wave can arrive at the moist layer with undiminished amplitude. However, the ascent corresponding to this wave is small—less than the estimated ascent for Phase I of GATE when rainfall remained unorganized. For larger values of the shear, this threshold can be exceeded, although the ascent decays beneath the jet. Thus, the question arises whether a wave source can organize rainfall from an arbitrarily large distance above the moist layer. It is suggested that organization can only occur if the unstable jet is within a few kilometers of the moist layer and separated by large shear, although exceptions are noted.

The calculation is applied to a wind profile resembling the observed 600-mb African jet. The wave amplitude decays beneath the jet so that the ascent at the top of the moist layer increases as the separation of the jet and moist layer decreases. Evidence is presented that the waves are closer to the moist layer during the late summer, resulting in larger ascent at this time.

Large variations in the ascent can also occur even if the separation of the jet and moist layer remains constant. It is shown that the ascent can vary greatly as a result of small changes in the jet that are within its observed summer variability.

1. Introduction

The organization of rainfall by African waves has led modelers to consider whether such waves could be driven by latent heat release, resulting in a class of models referred to as wave-CISK. However, as noted by Stevens and Lindzen (1978), among many others, wave-CISK models lack a preferred horizontal scale. The horizontal scale of the observed waves is not regarded as particularly mysterious. African waves originate in Central and East Africa (e.g., Carlson 1969b; Burpee 1972; Albignat and Reed 1980), upstream of the region where rainfall is organized (Carlson 1969a), and appear first within an easterly jet that was shown by Burpee (1972) to be unstable. The shear instabilities associated with the jet have horizontal scales comparable to those of the observed waves (Rennick 1976; Simmons 1977; Mass 1979; Kwon 1989). Thus, African waves apparently originate as shear instabilities, while organized latent heating can contribute to wave growth as the waves approach the buoyant monsoonal air near the West African coast (Mass 1979).

This was observed during Phase III of the GARP Atlantic Tropical Experiment (GATE) in late summer 1974. Rainfall near the West African coast was consistently organized by African waves so that enhanced precipitation coincided with the passage of the wave trough. However, African waves do not always organize rainfall. During Phase I, two months earlier, there was no consistent relationship between rainfall and wave passage (Reeves et al. 1979). While precipitation rates were comparable for the two phases (Woodley et al. 1983), during Phase I rain was as likely to fall over the wave ridge as over the trough.

In this study, we consider what determines whether African waves organize rainfall and, in particular, why rainfall remained unorganized during Phase I of GATE. Chen and Ogura (1982) show that while African waves were present within the 600-mb easterly jet during each

Corresponding author address: Dr. R. L. Miller, NASA/GISS, 2880 Broadway, New York, NY 10025.

observing phase of GATE, surface convergence was barely disturbed by the waves during Phase I, in contrast to Phase III. We will assume that African waves originate as shear instabilities of the 600-mb jet (hereafter referred to as the African jet), as is suggested by the observational analyses of Burpee (1972) and Norquist et al. (1977). We hypothesize that an African wave can organize rainfall if the shear instability is able to penetrate beneath the jet and converge sufficient amounts of moisture. We will consider what prevented African waves from penetrating into the moist layer with sufficient amplitude during Phase I.

The correlation between moisture convergence and rainfall is well documented for African waves (Thompson et al. 1979; Chen and Ogura 1982). Our assumption that moisture convergence *causes* deep convection and rainfall is also shared by the African wave models of Rennick (1976), Mass (1979), and Kwon (1989). We will assume that only moisture beneath approximately 800 mb can contribute to rainfall. This is roughly the depth of the moist, conditionally unstable, monsoonal air that flows over West Africa where African waves are first observed to organize rainfall (Carlson 1969a). Consequently, the total convergence of moisture is proportional to the ascent at the top of the layer.

Traditionally, the ascent associated with a shear instability has been estimated by means of linear stability analysis (e.g., Rennick 1976; Simmons 1977; Mass 1979; Kwon 1989). However, below the jet, unstable normal modes are associated with neutral waves propagating across the shear (cf. appendix A). We will regard the unstable jet as a wave source and specify the amplitude of the wave just beneath the jet, using the potential vorticity equation to compute its amplitude below (cf. Fig. 1). The extent of penetration will thus depend on the index of refraction and, in particular, the zonal wind in the layer separating the African jet from the moist layer. Our model is described in more detail in section 2. Our use of the potential vorticity equation resembles that of Charney and Drazin (1961), although we are interested in the ascent induced by the wave rather than the geopotential amplitude.

Before turning to the example of African waves, we examine the more general behavior of our model in section 3. In particular, we will consider which zonal-wind profiles allow a wave source to induce the largest ascent below and whether there is any maximum depth beyond which a wave source is incapable of organizing rainfall.

In section 4, we consider whether differences in the winds beneath the African jet might have reduced ascent and total converged moisture during Phase I in comparison to Phase III. We will consider a zonal-wind profile resembling the jet and show that small deviations from this profile within the observed summer variability could cause relatively large changes in the induced ascent. In addition, we will present evidence

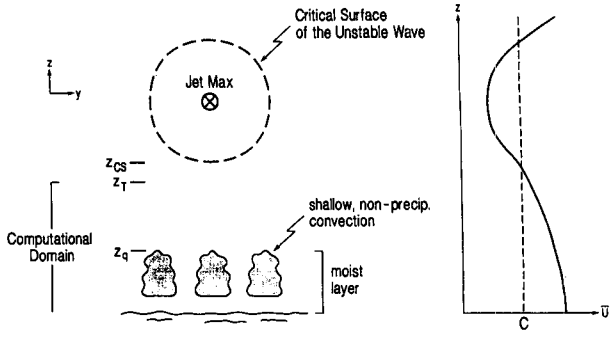

FIG. 1. A schematic view of a jet perched above a potentially buoyant moist layer. In the model, the amplitude, phase speed, and horizontal wavenumber of the unstable wave are specified at z_T, and the ascent induced by the wave below is computed as a function of the zonal wind at each height. Of particular interest is the ascent induced at z_q, the top of the moist layer. Here z_T is chosen to be just below z_{cs}, the lowest extent of the critical surface. In the example of African waves, the jet is centered near 600 mb, and the top of the moist layer is near 800 mb.

that variations in the jet allow larger ascent during late summer, when rainfall was most consistently organized. Finally, in section 5, we summarize our results.

How much moisture must be converged by a shear instability in order to organize rainfall remains to be determined. As a result of the converged moisture, latent heating will force a circulation with the same horizontal scale. This circulation has been modeled by Stevens and Lindzen (1978), who found that the convergence forced by latent heating is in phase and equal in amplitude to the original convergence. That is, the convergence forced by shear instability and latent heating reinforce each other, allowing latent heating to contribute to wave growth, as was observed during Phase III (Norquist et al. 1977). In principle, it seems that any nonzero amount of convergence resulting from the shear instability could lead to reinforcement and the eventual organization of rainfall. In practice, the situation is more complicated. For example, rainfall remained unorganized during Phase I, despite the presence of nonzero, albeit small, convergence due to the shear instability. Apparently, some threshold must be exceeded. We will return to this point in section 4. Whatever its precise value, the existence of a threshold makes it useful to consider what determines the amount of convergence within the moist layer that is induced by a disturbance originating within the unstable jet.

2. Model description

Our model is summarized in Figs. 1 and 2. We assume that as a result of shear instability, a wave with phase speed c and zonal wavenumber k propagates downward, away from the unstable jet. We specify the amplitude of this wave at z_T, the top of our computational domain, corresponding to a level just beneath the jet (cf. Fig. 1), and calculate the wave amplitude

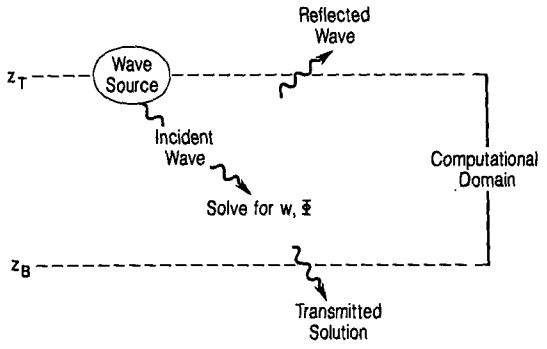

FIG. 2. A schematic view of the model.

below z_T, using the quasigeostrophic potential vorticity equation

$$\frac{\partial^2}{\partial y^2}\Phi + \frac{f^2}{N^2}\frac{\partial^2}{\partial z^2}\Phi + \mu^2(y, z)\Phi = 0, \qquad (1)$$

where

$$\mu^2 \equiv \left(\frac{\bar{q}_y}{\bar{U} - c} - k^2\right) - \frac{f^2}{4N^2H_0^2}, \qquad (2)$$

and the perturbation has been written in normal-mode form:

$$\Phi(x, y, z, t) = \Phi(y, z)e^{ik(x-ct)}e^{(z-z_T)/2H_0}.$$

Beneath the jet, the meridional shear is relatively small and μ^2 is mainly a function of height. (We will discuss this approximation in more detail.) Then, $\Phi(y, z)$ can be written as $\Phi(z)\sin ly$ and (1) becomes the wave equation:

$$\frac{\partial^2}{\partial z^2}\Phi + m^2(z)\Phi = 0 \qquad (3)$$

with an index of refraction that depends only on height:

$$m^2 \equiv \frac{N^2}{f^2}\left(\frac{\bar{q}_y}{\bar{U} - c} - k^2 - l^2\right) - \frac{1}{4H_0^2}. \qquad (4)$$

Given the geopotential at each level below the jet, we can use the thermodynamic equation to calculate the associated ascent:[1]

$$w = \frac{ik}{N^2}\left[\left(\bar{U}_z - \frac{\bar{U} - c}{2H_0}\right)\Phi - (\bar{U} - c)\Phi_z\right]e^{(z-z_T)/2H_0}. \qquad (5)$$

At z_B, the bottom of our computational domain, we impose the radiation condition so that the solution represents either a wave with downward group velocity or a downwardly decaying exponental. Our use of the radiation condition is intended to mimic the effects of dissipation near the surface, which acts to damp the downgoing solution and limit reflection. Presumably, this damping is overestimated by the radiation condition, which assumes that the wave excited above z_T is completely absorbed beneath z_B. At the other extreme is the kinematic condition (i.e., w is set equal to zero), where the surface acts as a perfect reflector. It is unclear which condition more accurately describes the degree of reflection. Although we have chosen to implement the radiation condition, we will consider the sensitivity of our conclusions to this choice in section 4.

The model requires that phase speed and horizontal structure of the instability be specified at the top of the computational domain. That is, we implicitly assume that these parameters are determined within the jet and *above* the computational domain. Calculations by Shukla (1979) and Goswami et al. (1981) suggest that our assumption is valid to a good approximation. Both studies considered the stability of the zonal winds over the Bay of Bengal and demonstrated that the (complex) phase speed c and the horizontal structure were determined primarily by the properties of the unstable jet, while the neighboring winds and boundary conditions were of secondary importance. More recently, Kwon (1989) has shown that this is also true for the African jet, even though the structure of the unstable wave along with the wave energetics may depend strongly on the winds surrounding the jet.

This raises the question of precisely where z_T, the top of our computational domain, is to be located relative to the jet. By assumption, z_T is beneath the region of wave excitation, where the phase speed and horizontal structure are determined. A wave overreflection description of shear instability (e.g., Lindzen 1988) indicates that this region is bounded approximately by the critical surface where $\bar{U} = c_r$. Thus, in order to study the penetration of waves beneath an easterly jet, we should place z_T, the top of our domain, at a height where $\bar{U} - c_r > 0$. How far below the critical surface z_T should be placed is a matter of judgement since this surface is only an approximate boundary. To be conservative, we could take $\bar{U}(z_T) - c_r$ to be large. However, the goal is to measure wave penetration beneath the jet; therefore, to make $\bar{U}(z_T) - c_r$ too large is to exclude part of the region of interest. In calculations not presented, we found that for large enough values of the shear—including those values observed beneath the African jet—the solutions are relatively insensitive to $\bar{U}(z_T) - c_r$ for values less than a few m s^{-1}. Given this insensitivity, we arbitrarily choose z_T to be that height where $\bar{U}(z_T) - c_r = 0.5$ m s^{-1}.

Our goal is to calculate how the ascent induced by a shear instability varies with the wind beneath the jet. According to (4), the ascent also depends on c_i, the imaginary part of the phase speed. This is inconvenient

[1] Synopticians customarily evaluate w using the Omega equation. However, for geopotential fields that are a solution to (3), the thermodynamic and omega equations give identical values of w (e.g., Holton 1979).

since the computed ascent will vary not only with the low-level winds, but also over the life cycle of the wave. In order to remove this dependence on c_i, we make use of the result derived in appendix A that within our domain the unstable normal mode is comprised of wave packets. In the appendix A it is shown that the individual packets propagate according to (3) but with c_i set equal to zero. In this study, the ascent associated with a wave packet rather than the normal mode is computed, since in the former case, this ascent depends only on the low-level wind. By computing the ascent corresponding to a wave packet, we are not approximating African waves as neutral (or slowly growing). In appendix A we show that while an individual packet is neutral, the summation over all the (neutral) packets that exist at any single instant can result in an unstable normal mode. Because the amplitude computed in this study corresponds to the wave packet, this amplitude and its variation with height cannot be compared to variations in the observed wave, since the latter corresponds to the superposition of all packets. An exception where such a comparison is approximately valid is where c_i is small, for example, over the GATE ship array in the east Atlantic, where African waves are observed to have equilibrated.

Derivation of a one-dimensional wave equation from (1) requires that the index of refraction be a function only of height: meridional variations of the index resulting from the meridional shear beneath the jet are assumed to be small. In section 4, we will justify this neglect by scale analysis and by direct comparison of the solutions to (1) and (3) for a wind profile resembling the African jet. As a result of this approximation, the meridional structure of the perturbation can be written as $\Phi(y, z) \propto \sin ly$. Such a perturbation has no meridional tilt and extracts no energy from the unstable jet. This may seem to contradict our assumption that the perturbation origin is due to shear instability—in particular due to a combination of baroclinic and barotropic instability. However, while the perturbation is assumed to have no tilt within our computational domain beneath the jet, we assume that within the jet (and thus above our domain) the perturbation has a tilt allowing it to extract energy from the shear. This picture is consistent with the meridional structure of African waves observed during Phase III of GATE. Reed et al. (1977) show that at 700 mb, near the jet core, the perturbation streamlines are meridionally tilted so that the wave grows at the expense of the jet. However, such a tilt, along with the corresponding extraction of energy, is absent at 850 mb. This latter height is representative of the computational domain.

To pose our approximation quantitatively, we note that the index of refraction may be treated as constant in the meridional direction if the scale of variation for the index is large compared to the meridional length scale of the perturbation—that is, if

$$\frac{1}{\mu}\frac{\partial \mu}{\partial y} \ll l. \tag{6}$$

In essence, our approximation is based on the method of multiple scales (e.g., Ioannou and Lindzen 1986) for which (6) is a measure of the approximation's validity. For now, we will assume that (6) is satisfied, and defer quantitative estimate until section 4 when we apply the results of our model to the African jet.

Finally, we consider the usefulness of the quasigeostrophic and β-plane approximations in describing wave penetration beneath a jet at 15°N. Stevens (1979) has shown that African waves are approximately controlled by linear dynamics. Quasigeostrophy is a valid approximation to the linearized equations if the Doppler-shifted wave frequency $k(\bar{U} - c)$ is small compared to the Coriolis parameter. Consequently, in the vicinity of the critical level where the difference $\bar{U} - c$ is small, the behavior of African waves is quasigeostrophic. To estimate more precisely how small this difference must be, we set k equal to 2×10^{-6} m^{-1} and evaluate f at 15°N: the ratio $[k(\bar{U} - c)/f]$ is less than unity for $\bar{U} - c$ less than 19 m s^{-1}.

The validity of the β-plane approximation requires that (β/fl) be small or that l be much greater than 6×10^{-7} m^{-1}. For comparison, a typical value of l in this study is 2×10^{-6} m^{-1}. Alternatively, it is noted that for this value of l, the ratio (β/fl) is less than unity beyond roughly 4° of the equator.

3. The ascent induced by a wave source aloft

In the next section we will estimate the low-level ascent induced by instabilities of the African jet. But first, we consider a broader range of zonal-wind profiles, not necessarily resembling the African jet, and examine the more general behavior of the model—considering, for example, which zonal-wind profiles result in the largest ascent and whether there is any distance beyond which a wave source is incapable of organizing rainfall.

a. Constant $\bar{U}$

For a zonal-wind profile without vertical shear, analytic solutions exist that aid in the interpretation of the solutions corresponding to more realistic basic states.

In the absence of shear, the index of refraction becomes

$$m^2 = \frac{N^2}{f^2}\left(\frac{\beta}{U_0 - c} - k^2 - l^2\right) - \frac{1}{4H_0^2}. \tag{7}$$

The vertical scale m^{-1} is large in regions of small static stability. In addition, this scale is directly proportional to the Coriolis parameter: vertically trapped disturbances in the tropics are confined to a narrower depth than their midlatitude counterparts. In Fig. 3, m^{-1} is

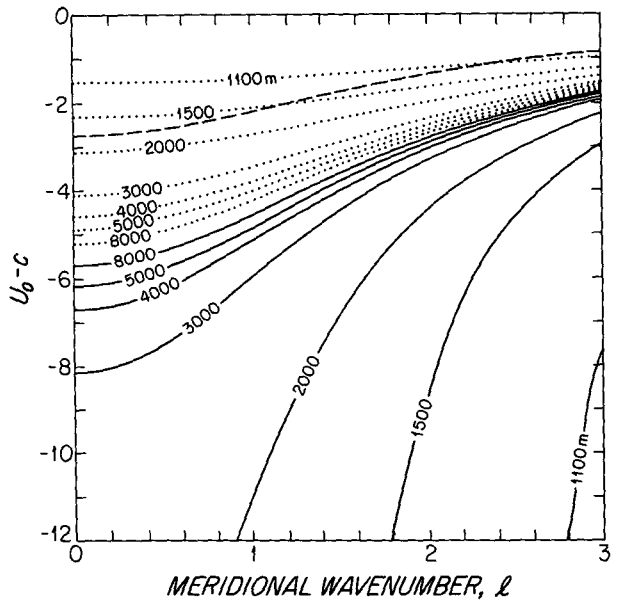

FIG. 3. The vertical length scale m^{-1} (in meters) as a function of the meridional wavenumber l ($\times 10^6$ m^{-1}) and $U_0 - c$ (in m s^{-1}). The solid lines correspond to vertically trapped solutions ($m^2 < 0$), where m^{-1} equals the e-folding scale; the dotted lines correspond to vertically propagating solutions ($m^2 > 0$), where m^{-1} equals the vertical wavelength divided by 2π; and the dashed line depicts the value of $U_0 - c$ that maximizes $|w|$ for the propagating solutions as a function of l.

plotted as a function of $U_0 - c$ and l. The other parameters required for this calculation are the zonal wavenumber k, which is given the synoptic-scale value of 2×10^{-6} m^{-1} (corresponding to a zonal wavelength of roughly 30° longitude), N^2, which is set equal to 1.16×10^{-4} s^{-2}, and f and β, which are evaluated at 15°N. (These values will be used throughout this study.)

According to (7), propagation ($m^2 > 0$) occurs within a range of $U_0 - c$ that is positive and small:

$$0 < U_0 - c < \beta \Big/ \left(k^2 + l^2 + \frac{f^2}{4H_0^2 N^2} \right). \quad (8)$$

This is the result of Charney and Drazin (1961): Rossby waves can propagate vertically if the zonal wind is slightly more westerly than the wave phase speed. For values of the parameters used in Fig. 3, vertical propagation occurs for $U_0 - c$ less than 2–3 m s^{-1}.

The vertical velocity associated with the perturbation can be calculated analytically in the absence of shear. For downward-propagating solutions, where $\Phi = \Phi_0 e^{-im(z-z_T)}$,

$$|w| = \frac{k}{N^2} (U_0 - c) m e^{(z-z_T)/2H_0} |\Phi_0|. \quad (9)$$

We are particularly interested in the maximum possible ascent associated with vertically propagating solutions, which can be found by varying $U_0 - c$. The maximum $|w|$ is

$$|w| = \frac{\beta}{2Nf} \frac{k}{\sqrt{k^2 + l^2}} e^{(z-z_T)/2H_0} |\Phi_0|, \quad (10)$$

which occurs for

$$U_0 - c = \frac{\beta}{2(k^2 + l^2)}.$$

The maximizing value of $U_0 - c$ as a function of l is denoted by the dashed line in Fig. 3.

By way of illustration we set $l = 2 \times 10^{-6}$ m^{-1} and $\Phi_0 = 23.5$ m^2 s^{-2}. (The latter value corresponds to a meridional wind of 1.25 m s^{-1}, which is comparable in magnitude to the shear instabilities beneath the African jet.) The optimal $|w|$ given by (10) is found to equal 0.17 mb h^{-1}.

This raises the question of how much convergence of moisture—or equivalently, how large a value of ascent at the top of the moist layer—is needed for a shear instability to organize rainfall. The optimal value of $|w|$ is small in comparison to the 3–5 mb h^{-1} ascent characterizing tropical convection averaged over a synoptic scale (e.g., Reed and Recker 1971; Thompson et al. 1979).

In the next section, we will argue that the ascent given by (10) is too small to organize rainfall beneath the African jet, since it fails to exceed an empirical threshold. However, under different circumstances, a vertically propagating wave may organize rainfall. Due to the linearity of (3) and (5), a wave source exciting a perturbation with sufficiently large initial amplitude would allow the threshold to be exceeded.

Restricting ourselves to perturbation amplitudes comparable to African waves, we find that the ascent associated with vertically propagating solutions is insufficient to organize rainfall. In contrast, the ascent associated with trapped solutions can exceed the aforementioned threshold, given a sufficiently large value of $U_0 - c$:

$$|w| = \frac{k}{N^2} (U_0 - c) \left(n + \frac{1}{2H_0} \right) e^{[n + (1/2H_0)](z-z_T)} |\Phi_0|,$$

where $\Phi = \Phi_0 e^{n(z-z_T)}$, and $n^2 \equiv -m^2$. The ascent corresponding to trapped solutions decreases exponentially beneath the wave source. Consequently, we question whether a wave insufficiently near the moist layer can organize rainfall.

The inability of a vertically propagating solution to organize rainfall distinguishes our calculation from that of Charney and Drazin (1961). Charney and Drazin considered whether a geopotential perturbation at one level in the atmosphere could be transmitted to another level with undiminished amplitude; for example, whether tropospheric geopotential anomalies could be transmitted into the stratosphere. According to (3), it

is sufficient to determine whether the zonal wind allows propagation between the two levels in question. In the present study, we consider whether a geopotential perturbation at one level can induce large *ascent* at another level, in particular at the top of the moist layer. In the example of the African jet, we find that the ascent associated with vertical propagation is insufficient to organize rainfall. Only profiles corresponding to trapping allow the threshold to be exceeded.

b. General $\bar{U}$

Based on the previous calculation, we suggested that only a wave source sufficiently near the moist layer could organize rainfall. We will demonstrate this using more realistic wind profiles with vertical shear and curvature. In addition, the maximum separation of the wave source and moist layer for which the threshold value can be exceeded will be estimated, and the wind profiles that allow the perturbation to induce the largest ascent will be identified.

Having turned to more realistic zonal-wind profiles, we now have to decide exactly how we want $\bar{U}$ to vary. Because it is impractical to solve (3) while varying $\bar{U}$ according to every possible combination of shear, curvature, and higher derivative, we cannot answer any of the preceding questions definitively. The difficulty lies in the fact that no convenient analytic solutions to (3) exist for general $\bar{U}$, so that the problem must be approached numerically.

In the interest of establishing a practical limit to the numerical calculations, we will consider zonal winds with overall easterly shear and only linear or quadratic dependence on height. In less specific terms, we will restrict our examination of vertical transmission to "smooth" profiles that might be found beneath an easterly jet. The reason for considering quadratic profiles in addition to the linear case is that for the former, the zonal wind can modify the index of refraction not only through the value of $\bar{U} - c$ as in the cases of constant and no shear, but also through the meridional gradient of mean potential vorticity $\bar{q}_y$.[2] The transmission will be different for linear and quadratic wind profiles because of this effect, even if each profile has identical overall easterly shear.

Before considering more complicated profiles, it is noted that because (3) and (5) are linear, the amplitude of the ascent will depend on the amplitude of the downgoing wave specified at the upper boundary. In order to compare the ascent corresponding to different profiles in a consistent fashion, it is necessary to identify the upgoing and downgoing components of the perturbation at z_T without resort to an approximation such as WKB, whose validity will vary according to the profile. As such, we invent a profile above z_T and below z_B, the lower boundary, that satisfies

$$\frac{\bar{q}_y}{\bar{U} - c} \equiv a_T^2, a_B^2$$

where a_T^2 and a_B^2 are constants, chosen so that m^2 is continuous at z_T and z_B. In addition, $\bar{U}$ and its first two derivatives are continuous across these points. The invented profile has the convenient property that m^2 is constant. As such, the appropriate radiation conditions can be imposed exactly at each boundary, without relying on the validity of the WKB approximation.

c. Linear $\bar{U}$

Given a linear wind profile, $\bar{U} = U_0 + U_1(z - z_T)$, (3) and (5) are solved numerically for the geopotential height and the vertical velocity.

The geopotential is depicted in Fig. 4 as a function of the shear parameter U_1 and the distance beneath the wave source $z - z_T$. The quantity $U_0 - c$ is set equal to 0.5 m s^{-1} for the remainder of this study. We have found that the trapped solutions in particular are insensitive to this parameter, the main effect of its variation being to shift the height of the turning point. The meridional wavenumber is set equal to 2×10^{-6} m^{-1}.

Qualitative aspects of the geopotential solution can be interpreted in terms of vertical propagation and trapping using the WKB approximate solution to (3), along with Fig. 3, which shows how the vertical wavenumber varies with respect to $\bar{U} - c$. For small values of the shear, (-0.5 m s^{-1} km^{-1} $< U_1 < 0$), the perturbation is simply a downward propagating wave, since the index of refraction is positive at all heights within our computational domain. For larger values of shear, the downgoing wave encounters a turning point above which a reflected wave returns to z_T and below which the perturbation is a downward decaying exponential.

One effect of the shear is to amplify the perturbation near the turning point. The most noticeable example occurs for $|U_1|$ slightly greater than 0.5 m s^{-1} km^{-1}, where the perturbation reaches an amplitude of 3.2 (normalized with respect to the amplitude of the downgoing wave at z_T) at 2 km below z_T. For comparison, if the perturbation was the sum of an incident and reflected wave in an environment without shear, the magnitude of the perturbation would be at most 2. The effect of shear in this example is to amplify the perturbation by a factor of roughly 1 1/2.

This amplification resembles the Airy-function behavior of the WKB solution, which varies as $(m^2)^{-1/4}$ outside the neighborhood of the turning point. Thus, as m^2 decreases toward this level, the wave amplitude increases. The physical interpretation for such an increase is that the vertical flux of wave action must re-

[2] Strictly speaking, $\bar{q}_y$ is modified by linear as well as quadratic profiles. However, this modification is much smaller for the former, given the range of shears we will consider.

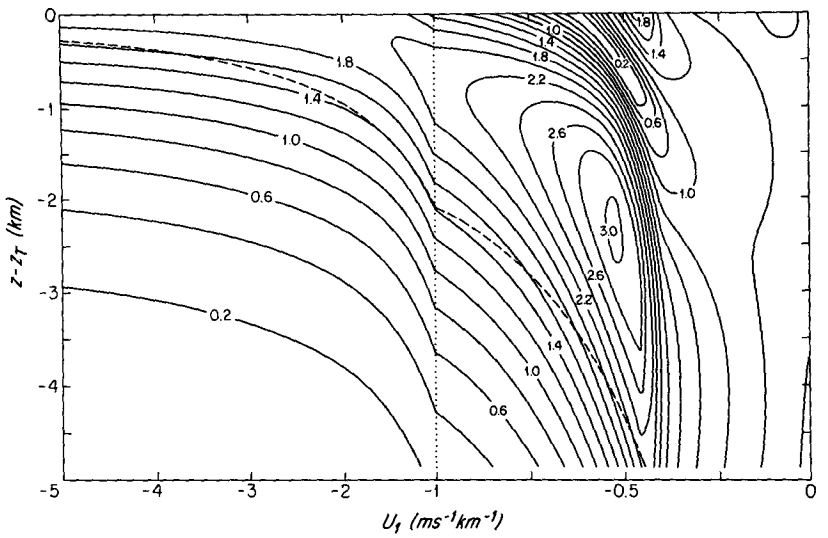

FIG. 4. The amplitude of the geopotential (normalized by the geopotential of the downgoing wave at z_T) as a function of distance beneath the wave source at z_T and the shear U_1. Note the expanded ordinate for -1 m s^{-1} < U_1 < 0. The dashed line corresponds to the turning point where the index of refraction passes through zero. $z_B = z_T - 5$ km.

main constant (e.g., Andrews et al. 1987). For solutions to (3), the product of the wave action (equal to the wave energy divided by the frequency) and the vertical group velocity is proportional to mA^2, where A is the wave amplitude. The constancy of this flux is equivalent to the requirement that $A \propto (m^2)^{-1/4}$.

For larger shears ($|U_1| > -2$ m s^{-1} km^{-1}), the turning point occurs within a kilometer of the upper boundary. These perturbations are trapped and have significant amplitudes only within a few kilometers of the wave source. For large values of U_1, the geopotential approaches an asymptotic form nearly independent of this parameter. This can be understood with reference to the calculation in the absence of shear. For large values of $U_0 - c$, the e-folding scale becomes nearly constant. Thus, for large values of U_1 (so that $U_0 - c$ is large), the solution below the turning point is a downward decaying exponential whose e-folding scale is nearly independent of $\bar{U}$.

The vertical velocity associated with the perturbation is shown in Fig. 5 (Φ_0 has been set equal to 23.5 m^2 s^{-2}). The smallest ascent is associated with small

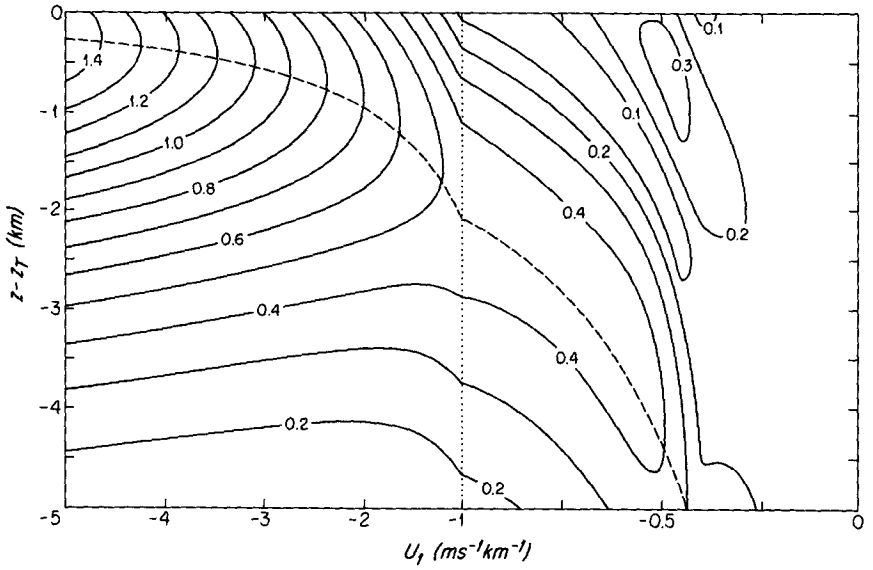

FIG. 5. Same as in Fig. 4 but showing the magnitude of the vertical velocity $|w|$ in mb h^{-1}.

values of the shear permitting vertical propagation. Based on empirical considerations, we suggest in section 4 that rainfall can be organized only if the perturbation ascent exceeds a threshold of 0.7 mb h^{-1}. For the range of shear used to construct the figure, the induced ascent exceeds the threshold only within 2 km of the wave source and for values of the shear greater in magnitude than roughly 2 m s^{-1} km^{-1}. Note that according to (5), the ascent is proportional to the vertical shear so that the ascent at any height can be made arbitrarily large given sufficiently large shear. As such, the maximum distance beneath z_T, within which the threshold is exceeded, depends on the largest shear we are willing to regard as "realistic," in addition to the magnitude of the wave source.

d. Quadratic $\bar{U}$

In the example of a linear profile, it was found that the induced ascent falls below an empirical threshold at distances greater than 2 km beneath the wave source. A quadratic term will be added to $\bar{U}$ so that $\bar{U} = U_0 + U_1(z - z_T) + U_2(z - z_T)^2$, and we will consider whether the induced ascent is modified by the addition of curvature. In particular, we will ask whether curvature allows the ascent to exceed the threshold at a greater distance from the wave source.

Figure 6 shows the largest value of $|w|$ occurring between z_T and z_B, while the height at which it occurs is given by Fig. 7. The horizontal axis in each figure corresponds to

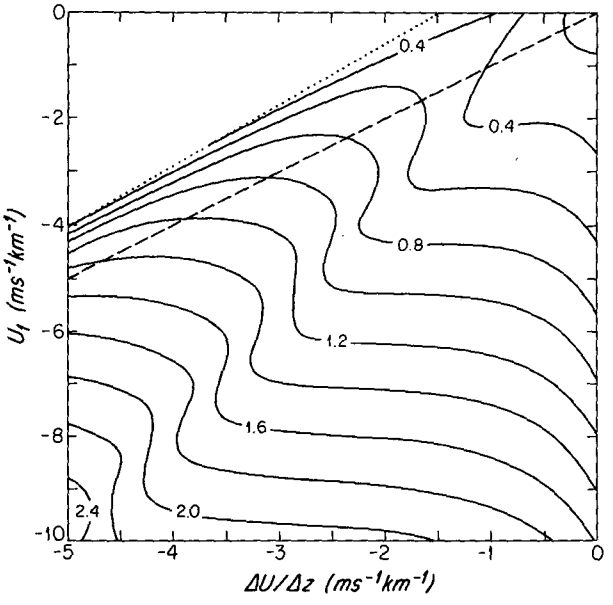

FIG. 6. The maximum value of $|w|$ in mb h^{-1} found between z_T and z_B, as a function of the vertically averaged shear $\Delta U/\Delta z$, and U_1, the shear at the upper boundary: $\Delta z \equiv z_T - z_B = 2$ km.

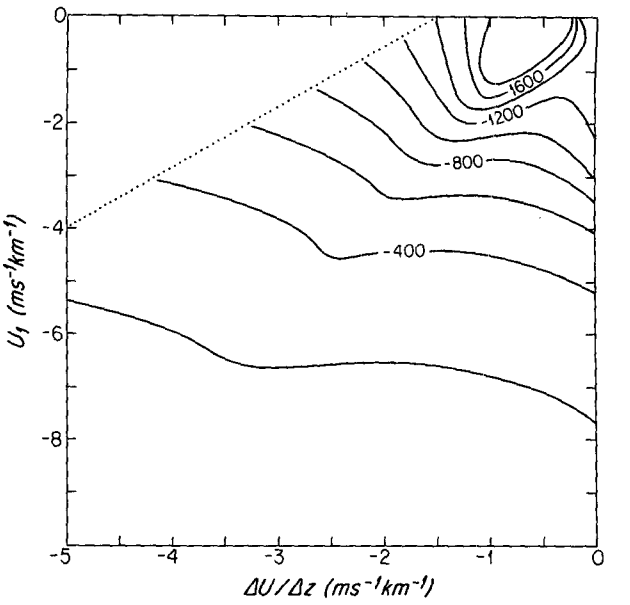

FIG. 7. The height at which the maximum value of $|w|$ in Fig. 6 is found.

$$\frac{\bar{U}(z_T) - \bar{U}(z_B)}{z_T - z_B} \equiv \frac{\Delta U}{\Delta z},$$

the average shear between z_T and z_B, while U_1, the shear at z_T, is plotted along the vertical axis. The dashed line in each figure corresponds to $U_1 = \Delta U/\Delta z$. These are profiles with no curvature so that along this line the maximum value of $|w|$ and the height at which it occurs correspond to those in Fig. 5. Since the curvature is equal to

$$2U_2 = \frac{2}{\Delta z}\left(U_1 - \frac{\Delta U}{\Delta z}\right),$$

regions of the figure below the dashed line correspond to profiles with negative curvature, while the curvature is positive above.

The presence of negative curvature allows larger values of w in comparison to linear profiles with the same average shear, according to Fig. 6. For example, while the largest ascent found using a linear profile is 1.4 mb h^{-1}, ascent up to twice this value is present below the dashed line in the figure. This might have been anticipated with reference to the thermodynamic equation (5), where the ascent is proportional to the vertical shear: profiles with curvature have local values of the shear exceeding $\Delta U/\Delta z$, the shear of the corresponding linear profile. For profiles with negative curvature, the shear is largest at z_T, near the maximum of Φ. Thus, the largest ascent in Fig. 6 is found for profiles with negative curvature.

An additional effect of curvature is to modulate the index of refraction through $\bar{q}_y$. This allows the possi-

bility that propitious values of curvature can minimize the decrease of the ascent beneath z_T by maintaining a generally positive index of refraction despite the increase of $\bar{U} - c$ beyond the range given by (8). In Fig. 8, the largest ascent at 2 km beneath z_T is for values of U_1 and $\Delta U/\Delta z$ where $m^2(z_B)$ is positive (Fig. 9). However, it is noted that according to (5), large ascent far below the wave source depends not only on Φ preserving its amplitude—requiring a positive and slowly varying index of refraction—but on $\bar{U}_z$, or $\bar{U} - c$, being large as well. Apparently, the largest ascent in Fig. 8 corresponds to combinations of shear and curvature that most nearly allow both of these constraints to be satisfied given the quadratic form of $\bar{U}$.

That certain values of negative curvature minimize the perturbation decay below z_T suggests that the addition of curvature can extend the distance beneath the wave source within which the induced ascent exceeds the threshold value. One can show by direct calculation that the threshold of 0.7 mb h^{-1} can be exceeded at up to 3½ km beneath the wave source, for roughly the same values of $\Delta U/\Delta z$ and U_1 corresponding to the largest ascent in Fig. 8.

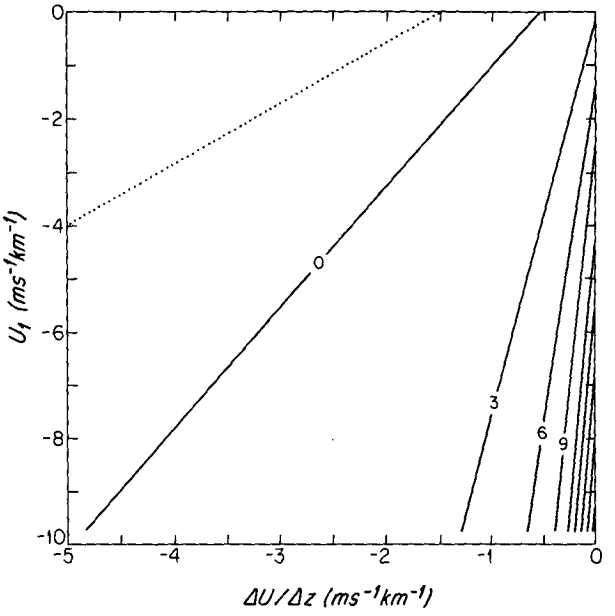

FIG. 9. The index of refraction ($\times 10^6$) at z_B for $\Delta z = z_T - z_B = 2$ km.

e. Summary

We have found that perturbations in the presence of shear and curvature can induce significantly larger ascent than if $\bar{U} - c$ were to lie within a small range described by (8), the Charney–Drazin inequality, wherein vertical propagation is allowed. To be sure, this statement depends on the height beneath the wave source at which one measures ascent. While a wind profile with shear and curvature allows substantially greater ascent to be induced near the source, this ascent decays with height in comparison to profiles satisfying (8), where the magnitude of the ascent is constant. Thus, far enough from the wave source, the largest ascent occurs when $\bar{U}$ satisfies (8).

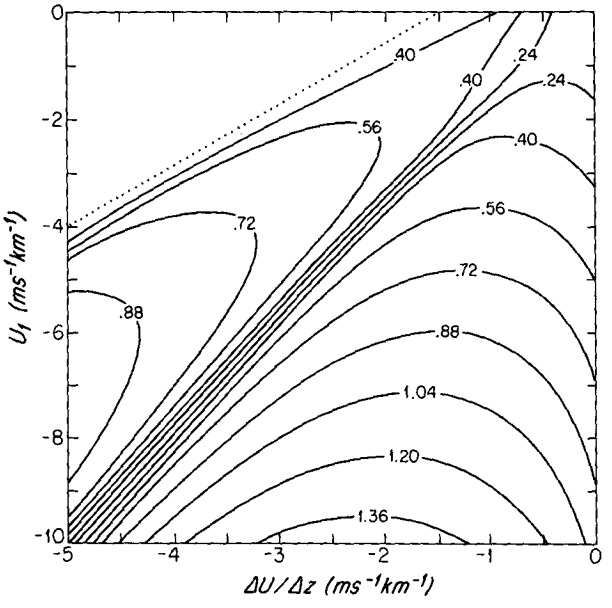

FIG. 8. The value of $|w|$ in mb h^{-1} at z_B, 2 km beneath the wave source, as a function of the vertically averaged shear $\Delta U/\Delta z$, and U_1, the shear at the upper boundary.

We have shown how the ascent in the case of weak shear is substantially less than the empirical threshold required for the organization of rainfall. However, this result depends on the strength of the wave source considered; hence, perturbations with amplitudes at z_T much larger than African waves can organize rainfall despite the weak shear. Otherwise, we have questioned whether a wave source can organize rainfall unless it is within a few kilometers of the moist layer and separated by sufficiently large shear. In addition to the amplitude of the wave source, this distance depends on the range of shear considered.

One might further question the universality of this distance since it is an estimate based on only three classes of wind profiles, namely, $\bar{U}$ equal to constant, linear, and quadratic functions of height. One nonpolynomial profile that might reasonably be expected to allow large ascent far from the wave source is suggested by a two-layer fluid where the zonal wind is discontinuous across the interface. In the lower layer, let $\bar{U} - c$ be constant and large so that near the top of this layer the ascent is large as well. In the upper layer, $\bar{U} - c$ is small enough so that propagation is allowed. Thus, one could imagine a wave source perched arbitrarily high within the upper layer, which despite its

distance from the interface induces large ascent in the lower layer.

However, the occurrence of such a configuration in the atmosphere is questionable. Clearly, the discontinuity in the zonal wind is unrealistic per se. Such a change in $\bar{U}$ must take place over a finite depth, which furthermore must be deep enough that the Richardson number remains everywhere greater than one-quarter. That the Richardson number constraint effectively precludes large ascent beneath the shear region, contrary to the implications of the two-layer model, is shown by Miller (1990).

The empirical approach of this study is inherently undefinitive. Nonetheless, it is our experience, based on low-order polynomials in addition to the nonpolynomial wind profiles described more fully in Miller (1990), that the results presented here are robust; namely, a wave source comparable in magnitude to the African jet can organize rainfall only if it is within a few kilometers of the moist layer.

4. Application to African Waves

While the rates of precipitation were comparable between Phases I and III of GATE (Woodley et al. 1980), rainfall was less frequently organized by African waves during Phase I in July of 1974. Sadler (1975) analyzed six years of satellite images and surface wind observations, finding that rainfall was most frequently organized in the late summer during these years as well. Observations of the jet-level winds were unavailable to Sadler, so it is unclear whether African waves were present during the entire season. However, Burpee (1972) analyzed upper-level wind observations over a different eight year period and found that wave amplitudes were comparable between the early and late summer. This suggests that the behavior observed during GATE is typical of other years: despite the occurrence of African waves and rainfall throughout the entire summer, rainfall is most frequently organized by the waves late in the season.

We assume that an African wave can organize rainfall if it is able to penetrate beneath the jet and converge sufficient amounts of moisture. During Phase III, surface convergence increased in phase with passage of the wave trough. In contrast, this field was barely disturbed during Phase I, despite the regular passage of African waves overhead (Chen and Ogura 1982). We will apply the model described in previous sections to estimate whether changes in the zonal wind beneath the jet might result in greater convergence toward late summer, and during Phase III in particular.

Ideally, we would have observations of the zonal wind just upstream of the region where rainfall is first organized by the waves. Carlson (1969a) notes that organization first occurs near the prime meridian. Unfortunately, this region is not well sampled by the GATE observing network. And measurements during Phase III over the ship array near 22°W indicate that the jet is 30% weaker than its zonal average across the entire GATE network (Chen and Ogura 1982; Reed et al. 1977). This suggests that there are significant zonal variations in the jet and that winds near the prime meridian may not be reliably estimated by downstream observations.

As an alternative, we will estimate the winds that exist in this region by referring to observations from other years. Wind observations at 5°E have been averaged by Burpee (1972) for eight successive months of August, while Mass (1979) repeated the analysis for the last week in August 1963. We will regard these analyses as representative of late-summer winds. We find that the induced ascent can be greatly altered by deviations from the profiles of Burpee and Mass that are within the observed summer variability, demonstrating that the convergence of moisture might vary greatly over the course of the summer.

We will suggest that variations in the observed zonal wind lead to increased convergence toward the late summer when rainfall is most frequently organized. However, the vertical resolution of the existing wind observations is probably insufficient to demonstrate this directly. The data available to Burpee and Mass consist of measurements at only the standard levels. That is, the winds beneath the African jet are characterized by observations at 700 mb, 850 mb, and the surface, so that the vertical shear and curvature—even the maximum intensity and height of the jet—are presumably not given with much accuracy. Evidence does exist, however, that the shear instabilities are closer to the moist layer during late summer: we will explain how this can result in greater convergence of moisture according to our model.

a. The transmission model applied to the African jet

Application of the model requires that we specify the level beneath the African jet corresponding to z_T, the top of our computational domain, along with the amplitude and horizontal structure of the shear instability at this height, and the zonal wind below.

The zonal wavenumber k is set equal to 2×10^{-6} m^{-1}, corresponding to a zonal wavelength of roughly 30° of longitude. This is within the range derived by synoptic and spectral analyses (e.g., Burpee 1972; Reed et al. 1977), and because our conclusions are not sensitive to this parameter we will not attempt to extract a more precise value from the observations.

As in the previous section, we will assume that the two-dimensional index of refraction μ^2 [cf., Eq. (1)] is approximately independent of latitude; therefore, we may express the meridional dependence of an African wave as $\Phi(y, z) \propto \sin ly$. We can judge the validity of our approximation by computing μ^2 for a profile re-

sembling the African jet and estimate the ratio in (6). Let

$$\bar{U} = U_0 \operatorname{sech}^2 \frac{y}{\Delta y} \cos^2 \frac{\pi(z - z_0)}{\Delta z}, \qquad (11)$$

where the quantities U_0, Δy, Δz, and z_0 are chosen so that the function $\bar{U}$ has horizontal and vertical shear and curvature comparable to observed values. In particular, we choose $U_0 = -16$ m s^{-1}, $\Delta y = 6.4°$ latitude, $\Delta z = 8$ km, and $z_0 = 4$ km. The computed index is shown in Fig. 10. Note that μ^2 changes rapidly with respect to latitude at the level of the jet, as required for barotropic instability (Lindzen and Tung 1978), and that the index of refraction is discontinuous at the critical surface. In contrast, the latitudinal variation of μ^2 beneath the jet is smaller. Our approximation of the African waves' latitudinal structure will be valid to the extent that this variation is small over the assumed meridional wavelength.

We take $l = 2 \times 10^{-6}$ m^{-1}, consistent with the observed meridional scale of African waves according to Reed et al. (1977). For comparison, one can estimate the scale of variation for the index of refraction and compute the ratio (6). At 500 m beneath the lower critical surface (corresponding to $z = 1.5$ km in Fig. 10), $\mu^{-1} d\mu/dy$ is approximately 1×10^{-6} m^{-1} near the central latitude of the jet while decreasing toward the wings. While this is not vanishing in comparison to l, it is nonetheless smaller, suggesting that vertical, rather than meridional, variations in the index of refraction are most fundamental to the convergence of moisture beneath the African jet. We will find by direct calculation that the solutions to (1) and (3) are not greatly different.

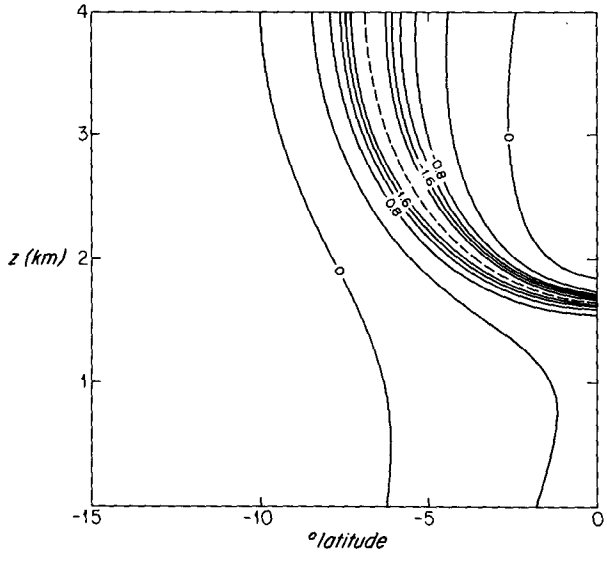

FIG. 10. The index of refraction ($\times 10^6$) for the jet described in the text. The index at heights above 4 km and at latitudes north of the jet can be constructed by symmetry. The dashed line represents the critical level where m^2 is singular. (Contours are not depicted for $|m^2| > 2 \times 10^{-6}$ m^{-2}.)

Next, z_T, the top of our computational domain, is assigned to an actual height in the atmosphere. As in the previous sections, we choose z_T to be that height where $\bar{U} - c$ equals 0.5 m s^{-1}, noting that the model solutions are relatively insensitive to this value for shears as large as those observed beneath the African jet. This corresponds to a height of roughly 800 mb during Phase III of GATE (Reed et al. 1977) near the top of the moist layer. We will argue below that z_T was possibly 100 mb higher during Phase I. Because of the large shear beneath the jet, z_T is within 10 mb of z_{cs} (cf. Fig. 1), and for the purposes of this study, we will regard z_T and z_{cs} as coincident.

At this level, the amplitude of the downgoing wave is chosen to correspond to a meridional wind of 1.25 m s^{-1}. The shear beneath the jet is large enough that the downgoing wave will encounter either an internal turning point or an abrupt change in the index of refraction, resulting in a reflected wave. As such, the meridional wind at z_T corresponding to the total perturbation will be somewhat less than 2.5 m s^{-1}. While this is comparable to the observed meridional wind at this height (Reed et al. 1977), based upon measurements during Phase III of GATE, it is noted that the amplitude of the downgoing wave in our calculation corresponds to an individual wave packet and not to the entire normal mode (which presumably is more closely related to the observed wave). According to appendix A, the amplitude of the wave packet is determined by the amplitude of the instability within the jet at the time the packet leaves the jet. Thus, while the advantage of a packet description of an African wave is that the ascent is independent of c_i—which varies over the life cycle of a wave—the disadvantage is that the packet ascent depends on the amplitude of the instability, which also varies along the wave's trajectory. Fortunately, this is not inconvenient so long as our conclusions can be phrased independently of the assumed initial packet amplitude. The value of the aforementioned wave amplitude will be used only for the sake of illustration.

The vertical shear and curvature beneath the African jet remain to be determined. In addition, we have to account for the contribution of $\bar{U}_{yy}$ to $\bar{q}_y$. As noted above, while $\bar{U}$ is in fact a function of latitude, changes in the index of refraction are small over the meridional scale of the wave, and we make the approximation of assigning to $\bar{U}_{yy}$ a single, representative value. Because the African jet is easterly, $\bar{U}_{yy}$ is positive and diminishes $\bar{q}_y$, although the diminution decreases as $\bar{U}$ decreases beneath the jet. In appendix B, evidence is presented that $\bar{q}_y$ is positive beneath the lower critical surface and z_T, despite the negative contribution of $\bar{U}_{yy}$. The precise diminution of $\bar{q}_y$ by $\bar{U}_{yy}$ remains uncertain. For the moment, we will assume that $\bar{U}_{yy}$ is negligible com-

pared to β. When we turn to the full potential vorticity equation (1), we will consider how a more realistic value of $\bar{U}_{yy}$ affects the solution.

Finally, we estimate the vertical shear and curvature beneath the African jet. The analysis of Burpee (1972) suggests an overall shear of -10 to -15 m s^{-1} over 3½ km. Mass (1979) questioned whether averaging over such an extended period of time might result in a smoother jet than is actually presented to the developing wave. He repeated Burpee's analysis for the last week of August 1963 and found the change in $\bar{U}$ between the jet maximum and the surface within the range of -15 to -20 m s^{-1}. [This estimate of the average shear includes the contribution from the low-level westerly flow that Mass omitted from his Fig. 4 flow shown by Sadler (1975) to be a consistent feature throughout the summer.] From these analyses, it appears that $-\Delta U/\Delta z$ is equal to 4–5 m s^{-1} km^{-1}. This range may underestimate the shear in certain instances; Carlson (1969a) has noted that the overall shear can be as large as 40–50 kt over 3 km, corresponding to $\Delta U/\Delta z$ as large as -8.6 m s^{-1} km^{-1}. Carlson did not mention how common or long lived such large shears were, however, or whether they included a contribution from the wave.

The curvature is harder to estimate, given the lack of vertical resolution in climatic datasets. According to Burpee and Mass, the shear is largest near the lower critical surface—probably no larger than twice the overall shear—so that the curvature is negative beneath this height. The existence of negative curvature is consistent with the analysis of Reed et al. (1977), who show that during Phase III of GATE the meridional temperature gradient was largest near 800 mb.

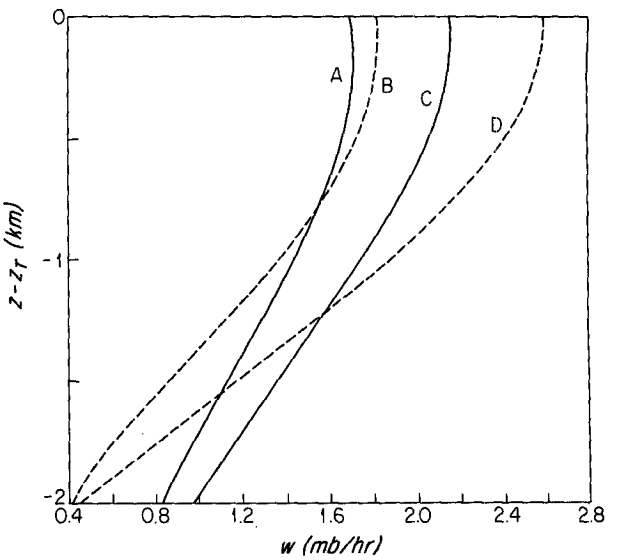

FIG. 12. The ascent in mb h^{-1} corresponding to the four profiles in Fig. 11.

b. Results

Four zonal-wind profiles within the range of shear and curvature discussed in subsection 4a are shown in Fig. 11. While differences between the profiles might be hard to measure, the corresponding ascent and geopotential fields, depicted in Figs. 12 and 13, respectively, are easily distinguished. In comparison to the

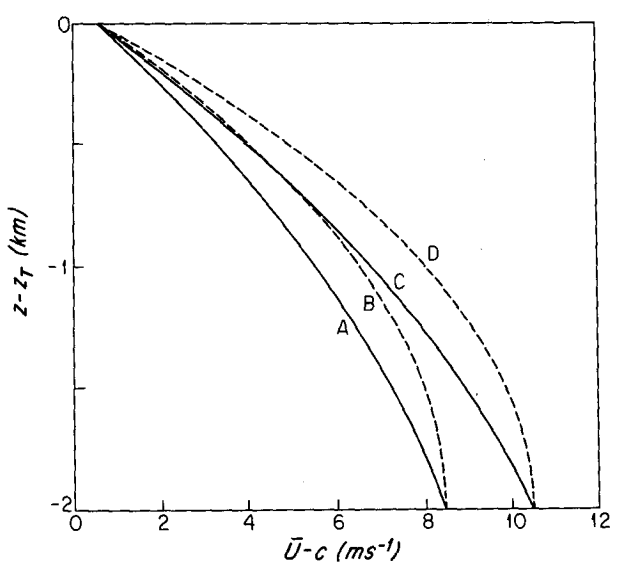

FIG. 11. Four zonal-wind profiles resembling the African jet. For curve A, $\Delta U/\Delta z = -4$ m s^{-1} km^{-1} and $U_1 = 1.5\Delta U/\Delta z$; curve B, $\Delta U/\Delta z = -4$ m s^{-1} km^{-1} and $U_1 = 2.0\Delta U/\Delta z$; curve C, $\Delta U/\Delta z = -5$ m s^{-1} km^{-1} and $U_1 = 1.5\Delta U/\Delta z$; and curve D, $\Delta U/\Delta z = -5$ m s^{-1} km^{-1} and $U_1 = 2.0\Delta U/\Delta z$. $\Delta z = 2$ km.

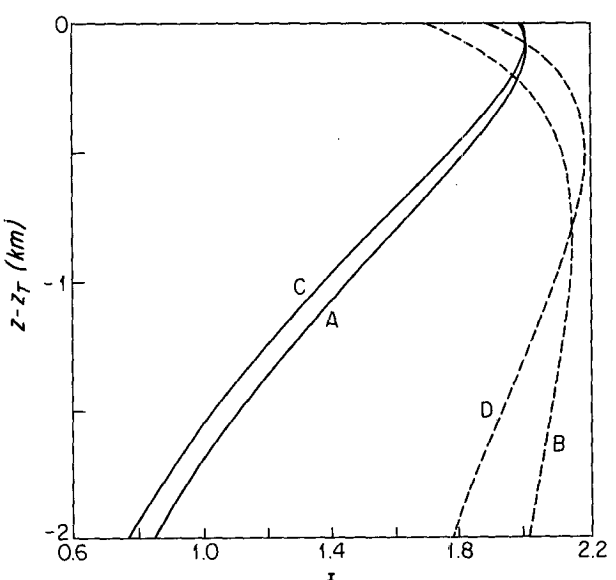

FIG. 13. The geopotential (normalized by the amplitude of the downgoing wave at z_T) corresponding to the four profiles in Fig. 11.

ascent associated with profile A, for example, the ascent corresponding to profile D is one and a half times larger near z_T, but only half as large at 2 km below z_T. Note that for profiles B and D, the decay scale for the geopotential differs from that of the ascent. This resembles a feature of African waves found by Chen and Ogura (1982) for Phase I of GATE; namely, the wave vorticity (proportional to the geopotential for quasigeostrophic perturbations) was virtually undiminished between the jet level and the surface, while the surface convergence (related to the vertical velocity) remained relatively unorganized by the wave. Incidentally, the index of refraction for profile B (Fig. 14) is positive over the entire 2-km depth, despite the change in $\bar{U}$ by 8 m s^{-1}. This demonstrates that propagation can occur even if $\bar{U} - c$ does not remain within the small westerly range given by (8), so long as the effect of curvature is to maintain a positive index of refraction.

Differences between the profiles in Fig. 11 are within the range of observations of the African jet (e.g., Burpee 1972; Reed et al. 1977; Chen and Ogura 1982). We regard this range as a conservative measure of the jet's variability over the course of the summer. As such, summertime variations in the induced ascent and the waves' ability to organize rainfall are potentially as large as substantial variations in the ascent shown in Fig. 12.

Whether these variations would result in larger ascent during the late summer—and Phase III in particular—when rainfall is most frequently organized, is harder to demonstrate given the dearth of suitable wind observations. Chen and Ogura (1982) show that African waves (whose height we take to be indicated by the vorticity maximum) are roughly 100 mb higher during Phase I of GATE in early July in comparison to Phase III in early September (their Figs. 24 and 25). This is significant insofar as the ascent corresponding to each of the wind profiles depicted in Fig. 11 ultimately decays in amplitude away from the jet. Consequently, the ascent induced at the top of the moist layer would increase toward the late summer, when the waves are closer to this region. Unfortunately, the analyses of Chen and Ogura may not be completely relevant to our model, since as noted in subsection 4a, they are based on observations taken some 20° of longitude downstream of where the waves first organize rainfall. Thus, by the time African waves reach the ship array, the original shear instability may have been obscured by the circulation forced by organized latent heating, at least during Phase III. Nonetheless, it is not unreasonable that the unstable waves might originate at a higher level during the midsummer, for example during Phase I. This is the time of year when the surface thermal gradient responsible for the African jet might be expected to have penetrated farthest into the troposphere. According to the thermal wind relation, the jet maximum occurs at the height where the thermal contrast falls to zero. Thus, the unstable waves would be perched at their greatest elevation during midsummer. This is further corroborated, albeit indirectly, by the midsummer decrease in wave amplitude at 700 mb, found by Burpee (1972). While one interpretation is that the waves are weakest during this time, this seems surprising since the African jet might be expected to be most unstable during the midsummer when the surface thermal gradient is strongest. An alternative explanation is that the shear instability remains of undiminished amplitude, but is farthest above the moist layer during the midsummer. Due to the trapped nature of the solutions, the wave amplitude at any fixed level beneath the jet decreases as the separation of the unstable wave from that level increases. Were the winds beneath the African jet to resemble profiles A and C, then elevating the jet by as little as 100 mb could account for the decrease in wave amplitude measured by Burpee. While not entirely definitive, the analyses of Chen and Ogura (1982) and Burpee (1972), along with our heuristic argument that the African jet should be higher during the midsummer, suggest that the induced ascent might be larger toward late summer, when rainfall is most frequently organized. Incidentally, our interpretation of the midsummer amplitude decrease found by Burpee illustrates that it may be misleading to measure wave amplitude as a function of time based on observations at a single level. This is particularly true for tropical disturbances where the trapping scale is small in comparison to midlatitudes.

The radiation condition has been used in the calculations presented up until now. We repeated the calculations leading to Figs. 11–14, this time setting w equal to zero at z_B (z_B again equals $z_T - 2$ km). As in Fig. 12, the ascent was again found to be sensitive to small changes in $\bar{U}$. The ascent decayed beneath z_T: in fact, the degree of trapping was greater than in Fig. 12, since w was necessarily zero at z_B, while w at z_T was largely unchanged by the new lower boundary condition. As discussed in section 2, our use of the radiation condition is intended to model the effects of dissipation near the surface. While it probably overestimates wave absorption, we note that use of the kinematic boundary condition (equivalent to no absorption) results in nearly identical behavior of the induced ascent.

Another approximation made in constructing Figs. 11–14 was the neglect of meridional variations in the index of refraction, μ^2 [cf. Eq. (1)]. To assess this approximation, we solved the full potential vorticity equation (1) to see to what extent the sensitivity of our solutions to the low-level wind was altered. The calculation was done using a β-plane centered at 15°N with channel boundaries at 0° and 30°N. As in the one-dimensional case, we imagined a downgoing wave propagating through the underside of the jet in the direction of the moist layer, and computed the wave am-

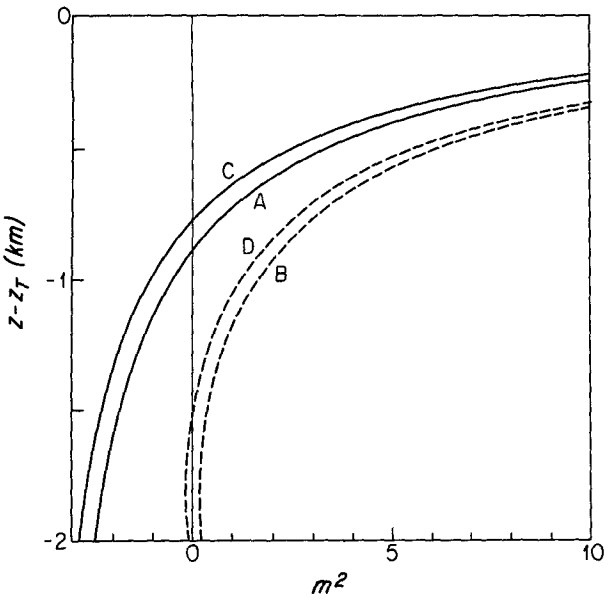

FIG. 14. The index of refraction ($\times 10^7$) corresponding to the four profiles in Fig. 11. Within 400 m of z_T, the index rises sharply, encountering a singularity at the critical level.

plitude at each height as a function of $\bar{U}$. The amplitude of the downgoing wave was chosen so that $\int_{y_s}^{y_n} \Phi^2(y, z_T)dy$ would be equal to the corresponding integral in the one-dimensional case: $\int_0^{\pi/l} \Phi^2(z_T) \sin^2 lydy$. At the lower boundary, either the radiation or kinematic condition was imposed. As before, the solutions were found not to depend greatly on this choice.

The vertical dependence of $\bar{U}$ was taken to be a quadratic function of height, as before. However, unlike the previous calculation, $\bar{U}$ also varied with latitude in proportion to $\text{sech}^2(y/\Delta y)$, so that $\bar{U}$ would resemble the underside of an internal jet [cf., Eq. (11)]. The quantity Δy was estimated from observations to be roughly 7°.

For 4 m s^{-1} km^{-1} $\leq -\Delta U/\Delta z \leq$ 5 m s^{-1} km^{-1} and $1.5\Delta U/\Delta z \leq U_1 \leq 2.0\Delta U/\Delta z$ (the same range used to construct Figs. 11–14), the solutions were again found to decay beneath z_T. The solutions to (1) also exhibited the same sensitivity to small changes in $\bar{U}$. In fact, the sensitivity was larger than depicted in Fig. 12. While the largest $w(z_T)$ in this figure is roughly one and a half times the smallest value, this ratio was found to be a full factor of two when (1) was used to calculate Φ and w. By neglecting meridional variations in the index of refraction, the sensitivity of w to $\bar{U}$ appears to be somewhat underestimated.

One feature was unique to the solutions of (1). For certain values of $\Delta U/\Delta z$ and U_1 within the range cited in the preceding paragraph, the largest values of ascent occurred not directly under the jet axis, but a few degrees of latitude to the north and south. This may be significant since, despite the idealized jet and moist layer depicted in Fig. 1, the moist monsoonal air that flows onto the West African coast has its northern boundary near the jet axis. Thus, wave ascent to the south may be more effective at organizing rainfall than the same ascent directly beneath the jet.

With this exception, the solutions to (1) generally reproduce the behavior found by assuming that the index of refraction varies only with height, although the sensitivity of ascent to $\bar{U}$ was found to be somewhat larger when this assumption was not made.

Our study has implications for the linear stability calculations applied to the African jet, as described by Rennick (1976), Simmons (1977), Mass (1979), and Kwon (1989). Kwon has argued that the energetics of the unstable waves depend on the assumed zonal wind. This is consistent with our results, where latent heating would presumably make a greater contribution to wave growth if the zonal wind beneath the jet were to allow the shear instability to converge greater amounts of moisture.

The earlier stability analyses also considered the question of whether the shear instability could force a significant fraction of the African wave ascent, or whether the large observed value was a consequence of latent heating associated with organized deep convection. That is, were African waves fundamentally different in their convergence fields from inviscid Rossby waves?

Rennick found that the shear instability could force a majority of the observed ascent, in contrast to the results of Mass and Simmons.[3] One possible source of the discrepancy is the differing numerical resolution used in each study. Rennick used five vertical levels, while Mass and Simmons had roughly twice that amount. We have found that for the 2-km layer depicted in Figs. 11–14, 21 points were needed in order for the solution to converge to within a few percent. Unfortunately, such resolution would be impractical in a two-dimensional calculation if the computational domain extended throughout the entire troposphere. For comparison, a 2-km layer would be represented by only 2 or 3 grid points in the models of Mass and Simmons.

Another possible reason for the discrepancy concerns the differing zonal-wind profiles used in each study. Although differences at the level of the jet may be germane, the discrepancy could also result from differences in $\bar{U}$ beneath the jet and the sensitivity of the wave-induced ascent, as described in this study.

Unfortunately, both of these reasons only point out

[3] The ascent published by Rennick is not noticeably different from the values given by Mass and Simmons. However, each calculation is linear so that the amplitude depends on how the eigensolution is scaled. Rennick's choice of scale is different from that used by Mass, and if both solutions are scaled consistently, the ascent corresponding to Rennick's solution increases significantly.

the difficulty and uncertainty inherent to such a calculation, without indicating whether the convergence field of an African wave really is different from that of a Rossby wave. In any case, we note that the moisture convergence associated with a shear instability derived from linear stability analysis will be systematically underestimated in comparison to the convergence of an African wave observed near equilibration (as in the case of the GATE observations). This is because, as described in appendix A, unstable growth results in exponential decay with respect to height of the wave amplitude away from the jet. This confinement of the wave within the jet lessens as the growth rate decreases. Thus, convergence outside of the jet (e.g., in the moist layer) will increase relative to the amplitude at jet level as the initial perturbation grows to observable amplitudes and approaches equilibration.

Finally, we return to the question of whether a wave source arbitrarily far above the moist layer can organize rainfall. In the previous section, we found that waves in the absence of shear could penetrate through deep layers with undiminished amplitude. However, the ascent corresponding to these solutions was small [cf., Eq. (10)], and we questioned whether it was sufficient to organize rainfall. That rainfall remained unorganized during Phase I despite the penetration, albeit weak, of the shear instability into the moist layer suggests that some nonzero value of ascent must be induced and that the Phase I ascent can provide a lower bound for the threshold.

Estimation of the Phase I ascent remains a somewhat uncertain process, since we know neither the precise form of the zonal wind beneath the African jet nor the distance separating the unstable wave from the moist layer. As an alternative, we can construct a plausible and generous range for these parameters and choose the smallest corresponding ascent to represent a lower bound.

The winds at 5°E, where the waves first organize rainfall, have been analyzed by both Burpee (1972) and Mass (1979). Both find that the lower critical surface is roughly coincident with the top of the moist layer near 800 mb. That is, $z_T - z_q \approx 0$, according to the nomenclature of Fig. 1. Both analyses are based on August wind observations, which are presumably more representative of Phase III winds than those of Phase I—especially the analysis of Mass that is based on the last week in August. During Phase I, $z_T - z_q$ might be larger, given that the waves were 100 mb higher over the GATE ship array in comparison to Phase III (Chen and Ogura 1982). In the interest of making a conservative estimate, we will take $z_T - z_q$ equal to 1500 m and search for the smallest ascent at this distance from the moist layer.

The overall shear lies within the range $4\ \text{m s}^{-1}\ \text{km}^{-1} \leq -\Delta U/\Delta z \leq 5\ \text{m s}^{-1}\ \text{km}^{-1}$, while U_1 is no more than twice $\Delta U/\Delta z$, according to Burpee and Mass. Given $z_T - z_q$, along with these ranges of $\Delta U/\Delta z$ and U_1, we find using either (1) or (3) that the smallest possible ascent during Phase I was near $0.7\ \text{mb h}^{-1}$. This in turn represents a lower bound for the threshold of ascent required for the organization of rainfall, which remained unorganized during Phase I.

This is much larger than the ascent given by (10), suggesting that a wave source can organize rainfall only if it is sufficiently close to the moist layer.

5. Conclusions

We have hypothesized that a shear instability can organize rainfall if it converges sufficient amounts of moisture, and we have calculated this convergence by specifying the amplitude of a downgoing wave just beneath the jet and calculating the ascent induced below as a function of the zonal wind.

Our results question whether a jet can organize rainfall from an arbitrarily large distance above the moist layer. While in the absence of shear, a wave can reach the moist layer with undiminished amplitude, the induced ascent is small—less than the estimated ascent during Phase I of GATE when rainfall remained unorganized. For larger values of the shear, this empirical threshold can be exceeded. However, these solutions decay beneath the wave source so that large ascent occurs within only a limited distance of the source. For an optimal combination of shear and curvature, we found that the induced ascent could exceed the threshold only if the wave source was within at most a few kilometers of the moist layer.

We have considered whether changes in the African jet could result in the waves' increased ability to organize rainfall during late summer, as observed during GATE. As a result of the large shear beneath the jet, the waves decay with respect to height so that the induced ascent increases as the distance separating the unstable wave from the moist layer decreases. Chen and Ogura (1982) show that the waves are roughly 100 mb closer to the moist layer during late summer. Unfortunately, their analyses are not entirely applicable to our model since they are based on observations taken over the GATE ship array, some 20° of longitude downstream of where rainfall is first organized. The African waves analyzed by Chen and Ogura reflect not only the shear instability that is central to our model but the circulation forced by latent heating as well, at least during Phase III. Nonetheless, their analyses are consistent with our suggestion that the unstable waves might be farthest above the moist layer during midsummer and, in particular, Phase I, when the surface thermal contrast responsible for the existence of the African jet has penetrated to its greatest height within the troposphere. This hypothesis would be relatively straightforward to test by the resumption of the wind-observing network over Central Africa that provided the data for Burpee's (1972) study.

Large changes in ascent can result even if the distance separating the unstable wave from the moist layer remains unchanged. Similar zonal-wind profiles, each closely resembling the observed winds, can result in values of the ascent that vary by up to a factor of 2. Whether the sensitivity of African wave ascent is as large as has been computed in this study may be difficult to assess, given the limited resolution of the wind observations. The analyses of Sadler (1975) suggest that late-summer organization of rainfall is a consistent feature of African waves. That the time of most frequent organization varies little from year to year may indicate that this sensitivity is not a feature of the observed waves and occurs in our model only due to some unrealistic simplification. For example, along-stream variations in the African jet perhaps cause the sensitivity found in our model to be "averaged out." On the other hand, this sensitivity may be masked in the observations by other effects. For example, if the African jet is higher during early summer, as we have hypothesized above, then this would reduce the sensitivity during the early summer that is indicated by our study, consistent with Sadler's analyses. In any case, it remains to be seen how the sensitivity we have found can result in systematically larger ascent toward late summer.

One aspect of our solutions can be verified by observations, namely, the decay of the ascent and geopotential fields with different vertical scales. For example, while the ascent associated with profile B in Fig. 12 fell to one-quarter of its value over 2 km, the magnitude of the geopotential remained relatively undiminished. This is reminiscent of the composite African wave during Phase I (Chen and Ogura 1982), where the wave vorticity decayed only slightly between the jet and the surface, in contrast to the wave convergence.

Our results have two implications for future studies. The first is that the curvature of the zonal wind must be measured accurately in order that the contribution of the shear instability to the total wave ascent be accurately calculated. We have noted how Rennick (1976) and Mass (1979) have come to opposite conclusions regarding this contribution despite their use of similar wind profiles (although this discrepancy might also result from the different vertical resolution used in each experiment). The estimation of curvature is made difficult by the practice of archiving rawinsonde data in terms of standard and significant levels, where the significant levels are defined so that the archived profile represents the actual winds only to within a linear interpolation.

Second, the calculation of wave amplitude as a function of time, based on observations at a single level, may be particularly misleading in the tropics where the vertical-trapping scale is relatively small. We have cited Burpee's (1972) finding that the African wave amplitude at 700 mb decreases during the midsummer. Due to the trapped nature of African waves, such a decrease may result from a wave of *undiminished* amplitude that is elevated by as little as 100 mb.

We have specified the downgoing wave amplitude immediately beneath the jet in order to calculate the convergence induced below. Since the calculation does not depend on the identity of the wave source, it also applies to the convergence within the moist layer forced by latent heating above this height. This equivalence may help us to understand why a threshold of convergence must be exceeded in order for an African wave to organize rainfall. The zonal-wind profile that limited the convergence induced by a shear instability during Phase I of GATE would also limit the convergence forced by latent heating. Perhaps the convergence resulting from the combination of the unstable jet and latent heating was insufficient to reinforce the heating during Phase I so that wave growth continued due to shear instability alone.

Acknowledgments. This work was supported by the National Science Foundation under Grant 8520354-ATM and the National Aeronautics and Space Administration under Grant NAGW-525. We thank Mike Rocha for drafting the figures. RLM thanks the NASA Goddard Institute for Space Studies for support while revising this article.

APPENDIX A

An Unstable Wave as the Sum of Neutral Wave Packets

In a slowly varying region, an unstable normal-mode solution to (3) is made up of two terms:

$$\Phi = e^{ik(x-ct)} \sin ly e^{\pm imz}$$
$$= e^{kc_i t} e^{ik(x-c_r t)} \sin ly e^{\pm imz},$$

where m is a slowly varying function of height, and m, k, and c are related by the dispersion relation,

$$m = m(k, c).$$

For the Rossby waves considered in this study, the dispersion relation is the equation defining the index of refraction:

$$m^2 = \frac{N^2}{f^2}\left(\frac{\bar{q}_y}{\bar{U} - c} - k^2 - l^2\right) - \frac{1}{4H_0^2}. \qquad (4)$$

Expand m in a Taylor series about $c = c_r$:

$$m = m(k, c_r) + \frac{\partial m}{\partial c}(c - c_r) + \cdots.$$

Use

$$\frac{\partial m}{\partial c} = \frac{\partial m}{\partial \omega}\frac{\partial \omega}{\partial c} = \frac{k}{c_{g,z}},$$

where $c_{g,z} \equiv \partial\omega/\partial m$ is the vertical component of group velocity. Then

$$m = m(k, c_r) + \left(\frac{k}{c_{g,z}}\right)c_i$$

so that

$$\Phi = e^{kc_i(t-z/c_{g,z})}e^{ik(x-c_r t)}\sin ly e^{\pm im(k,c_r)z}$$
$$\equiv A(t')e^{ik(x-c_r t)}\sin ly e^{\pm im(k,c_r)z}, \qquad (12)$$

where $A = e^{kc_i t'}$ and $t' \equiv t - z/c_{g,z}$.

Equation (12) can be interpreted as the response to a wave source with forcing amplitude A, which increases exponentially with respect to time. Following an individual wave packet (defined by $t' \equiv t_0'$, where t_0' is a constant corresponding to the time the packet leaves the wave source), A is constant. Thus, changes in the packet amplitude result only from variations of m in the factor $e^{\pm im(k,c_r)z}$. These variations are given by (4) so that m will change as a result of shear. For example, as $\bar{U} - c_r$ becomes large, m^2 becomes negative (i.e., m becomes imaginary) so that $e^{\pm im(k,c_r)z}$ corresponds to a trapped exponential. In any case, since $m(k, c_r)$ for an individual packet is evaluated from (4) with c_i set equal to zero, the packet behaves neutrally, even if it is part of an unstable normal mode.

Equation (12) can also be derived by evaluating m from (4), assuming that the quantity $c_i/(\bar{U} - c_r)$ is small. To summarize, (12) demonstrates that away from the critical surface [where $c_i/(\bar{U} - c_r)$ is not small] unstable normal modes are comprised of neutral waves.

At any instant in time, wave packets closest to the region of instability have originated most recently and are associated with larger values of t_0'. These packets begin with larger amplitudes than remote packets that originated earlier. Thus, the growing mode—which is the sum of all wave packets—decays away from the region of instability. This decay is in addition to any trapping associated with the individual wave packets—which results from the $e^{im(k,c_r)}$ factor. This confinement of the normal-mode amplitude to the region of instability is largest for large growth rates, where the difference in initial amplitude between successively forced wave packets is greatest.

Strictly speaking, the identification of unstable normal modes with neutral wave packets depends on the assumption of a slowly varying medium, which is not always formally satisfied. Nonetheless, Lindzen and Rosenthal (1981) and Ioannou and Lindzen (1986) have found that solutions to the Charney problem can be quite accurately approximated by a packet model based on vertically propagating waves, even for cases where WKB is not formally valid.

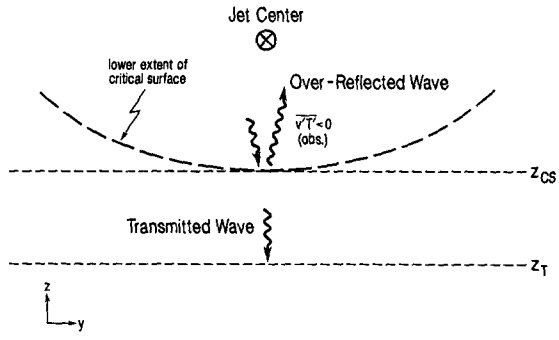

FIG. 15. A schematic view of overreflection from the lower part of the critical surface. The transmitted wave propagates into the computational domain at z_T.

APPENDIX B

Observational Evidence that $\bar{q}_y > 0$ beneath z_{cs}

The purpose of this appendix is to argue that $\bar{q}_y$ is positive beneath z_{cs} (cf. Fig. 1), the lower extent of the critical surface.

The observational evidence is indirect: Burpee (1972) and Reed et al. (1988) show that $\overline{v'T'}$ is negative near z_{cs}. That is, there is a down-gradient heat flux just above the critical surface. Using an argument similar to that in Lindzen and Tung (1978), we note that a down-gradient heat flux is equivalent to overreflection of waves incident on the critical level from the center of the jet [cf. Lindzen and Tung's Eq. (6)]. This situation is depicted in Fig. 15.

Overreflection at z_{cs} requires a "trapping" region, where the index of refraction is negative, immediately above z_{cs}. Since $\bar{U} - c$ is negative above z_{cs}, $\bar{q}_y$ must be positive. Thus, $\bar{q}_y$ is positive immediately above the critical surface. However, we do not expect $\bar{q}_y$ to pass through zero at z_{cs}; hence, $\bar{q}_y$ is presumably positive for some distance below z_{cs}.

There is additional evidence that $\bar{q}_y$ is positive beneath the lower extent of the critical surface. Reed et al. (1977) show that $\bar{U}_{zz}$ is negative beneath 800 mb, which corresponds to z_{cs} during Phase III of GATE. In this region, the horizontal curvature $\bar{U}_{yy}$ is the only term contributing negatively to $\bar{q}_y$. But Reed et al. (1977) calculate that $\beta - \bar{U}_{yy}$ is positive below 800 mb. This shows that $\bar{q}_y$ is positive below 800 mb since $\bar{U}_{yy}$ is not sufficiently large.

Admittedly, the last argument involves estimating second derivatives of $\bar{U}$, which is an uncertain computation. In contrast, the down-gradient heat flux measured by Burpee (1972) and Reed et al. (1988) is unambiguous, demonstrating indirectly that $\bar{q}_y$ is positive in the vicinity of z_{cs} and presumably for some distance below as well.

REFERENCES

Albignat, J. P., and R. J. Reed, 1980: The origin of African wave disturbances during Phase III of GATE. *Mon. Wea. Rev.*, **108**, 1827–1839.

Andrews, D. G., J. R. Holton, and C. B. Leovy, 1987: *Middle Atmosphere Dynamics.* Academic Press, 489 pp.

Burpee, R. W., 1972: The origin and structure of easterly waves in the lower troposphere of North Africa. *J. Atmos. Sci.*, **29,** 77–90.

Carlson, T. N., 1969a: Synoptic histories of three African disturbances that developed into Atlantic hurricanes. *Mon. Wea. Rev.*, **97,** 256–276.

——, 1969b: Some remarks on African disturbances and their progress over the tropical Atlantic. *Mon. Wea. Rev.*, **97,** 716–726.

Charney, J. G., and P. G. Drazin, 1961: Propagation of planetary-scale disturbances from the lower into the upper atmosphere. *J. Geophys. Res.*, **66,** 83–110.

Chen, Y.-L., and Y. Ogura, 1982: Modulation of convective activity by large-scale flow patterns observed in GATE. *J. Atmos. Sci.*, **39,** 1260–1279.

Goswami, B. N., V. Satyan, and R. N. Keshavamurty, 1981: Growth of monsoon disturbances over western India. *Monsoon Dynamics,* J. Lighthill and R. P. Pearce, Eds., Cambridge University Press, 415–428.

Holton, J. R., 1979: *An Introduction to Dynamic Meteorology.* Academic Press, 391 pp.

Ioannou, P., and R. S. Lindzen, 1986: Baroclinic instability in the presence of barotropic jets. *J. Atmos. Sci.*, **43,** 2999–3014.

Kwon, H. J., 1989: A reexamination of the genesis of African waves. *J. Atmos. Sci.*, **46,** 3621–3631.

Lindzen, R. S., 1988: Instability of plane-parallel shear flow (toward a mechanistic picture of how it works). *Pure Appl. Geophys.*, **126,** 103–121.

——, and K. K. Tung, 1978: Wave overreflection and shear instability. *J. Atmos. Sci.*, **35,** 1626–1632.

——, and A. J. Rosenthal, 1981: A WKB asymptotic analysis of baroclinic instability. *J. Atmos. Sci.*, **38,** 619–629.

Mass, C., 1979: A linear primitive equation model of African wave disturbances. *J. Atmos. Sci.*, **36,** 2075–2092.

Miller, R. L., 1990: Topics in shear instability: a) Viscous destabilization of stratified shear flow for Ri > 1/4; b) Organization of rainfall by an unstable jet aloft. Ph.D. thesis, Massachusetts Institution of Technology, 153 pp.

Norquist, D. C., E. E. Recker, and R. J. Reed, 1977: The energetics of African wave disturbances as observed during Phase III of GATE. *Mon. Wea. Rev.*, **105,** 334–342.

Reed, R. J., and E. E. Recker, 1971: Structure and properties of synoptic-scale wave disturbances in the equatorial Western Pacific. *J. Atmos. Sci.*, **28,** 1117–1133.

——, D. C. Norquist, and E. E. Recker, 1977: The structure and properties of African wave disturbances as observed during Phase III of GATE. *Mon. Wea. Rev.*, **105,** 317–333.

——, E. Klinker, and A. Hollingsworth, 1988: The structure and characteristics of African easterly wave disturbances as determined from the ECMWF Operational/Forecast System. *Meteorol. Atmos. Phys.*, **38,** 22–33.

Reeves, R. W., C. F. Ropelewski, and M. D. Hudlow, 1979: Relationships between large-scale motion and convective precipitation during GATE. *Mon. Wea. Rev.*, **107,** 1154–1168.

Rennick, M. A., 1976: The generation of African waves. *J. Atmos. Sci.*, **33,** 1955–1969.

Sadler, J. C., 1975: The monsoon circulation and cloudiness over the GATE area. *Mon. Wea. Rev.*, **103,** 369–387.

Shukla, J., 1977: Barotropic-baroclinic instability of mean zonal wind during summer monsoon. *Pure Appl. Geophys.*, **115,** 1449–1461.

Simmons, A. J., 1977: A note on the instability of the African easterly jet. *J. Atmos. Sci.*, **34,** 1670–1674.

Stevens, D. E., 1979: Vorticity, momentum, and divergence budgets of synoptic-scale wave disturbances in the tropical eastern Atlantic. *Mon. Wea. Rev.*, **107,** 535–550.

Stevens, D. E., and R. S. Lindzen, 1978: Tropical wave-CISK with a moisture budget and cumulus friction. *J. Atmos. Sci.*, **35,** 940–961.

Thompson, R. M., S. W. Payne, E. E. Recker, and R. J. Reed, 1979: Structure and properties of the synoptic-scale wave disturbances in the intertropical convergence zone of the Eastern Atlantic. *J. Atmos. Sci.*, **36,** 53–72.

Woodley, W. L., C. G. Griffith, J. E. Griffin, and S. C. Stromatt, 1980: The inference of GATE convective rainfall from SMS-1 imagery. *J. Appl. Meteor.*, **19,** 388–408.